

Photoacoustic radar phase-filtered spatial resolution and co-registered ultrasound image enhancement for tumor detection

Edem Dovlo,^{1*} Bahman Lashkari,¹ Andreas Mandelis,¹ Wei Shi,² and Fei-Fei Liu²

¹Center for Advanced Diffusion-Wave Technologies (CADIFT), Department of Mechanical and Industrial Engineering, University of Toronto, Toronto, ON M5S 3G8, Canada

²Ontario Cancer Institute, Princess Margaret Hospital, 610 University Ave., Toronto, ON M5G 2M9, Canada
*edovlo@mie.utoronto.ca

Abstract: Co-registered ultrasound (US) and frequency-domain photoacoustic radar (FD-PAR) imaging is reported for the first time in this paper. The merits of ultrasound and cross-correlation (radar) frequency-domain photoacoustic imaging are leveraged for accurate tumor detection. Commercial US imagers possess sophisticated, optimized software for rapid image acquisition that could dramatically speed-up PA imaging. The PAR image generated from the amplitude of the cross-correlation between detected and input signals was filtered by the standard deviation (SD) of the phase of the correlation signal, resulting in strong improvement of image spatial resolution, signal-to-noise ratio (SNR) and contrast. Application of phase-mediated image improvement is illustrated by imaging a cancer cell-injected mouse. A 14–15 dB SNR gain was recorded for the phase-filtered image compared to the amplitude and phase independently, while ~340 μm spatial resolution was seen for the phase PAR image compared to ~840 μm for the amplitude image.

©2015 Optical Society of America

OCIS codes: (170.5120) Photoacoustic imaging; (170.3880) Medical and biological imaging; (170.7170) Ultrasound; (170.7180) Ultrasound diagnostics; (100.0100) Image processing.

References and links

1. R. Siegel, J. Ma, Z. Zou, and A. Jemal, "Cancer statistics, 2014," *CA Cancer J. Clin.* **64**(1), 9–29 (2014).
2. M. Xu and L. V. Wang, "Photoacoustic imaging in biomedicine," *Rev. Sci. Instrum.* **77**(4), 041101 (2006).
3. S. Mallidi, G. P. Luke, and S. Emelianov, "Photoacoustic imaging in cancer detection, diagnosis, and treatment guidance," *Trends Biotechnol.* **29**(5), 213–221 (2011).
4. L. V. Wang and H. Wu, *Biomedical Optics: Principles and Imaging* (John Wiley & Sons, 2012), p. 376.
5. P. Beard, "Biomedical photoacoustic imaging," *Interface Focus* **1**(4), 602–631 (2011).
6. C. Li and L. V. Wang, "Photoacoustic tomography and sensing in biomedicine," *Phys. Med. Biol.* **54**(19), R59–R97 (2009).
7. R. A. Kruger, R. B. Lam, D. R. Reinecke, S. P. Del Rio, and R. P. Doyle, "Photoacoustic angiography of the breast," *Med. Phys.* **37**(11), 6096–6100 (2010).
8. P. Vaupel, F. Kallinowski, and P. Okunieff, "Blood flow, oxygen and nutrient supply, and metabolic microenvironment of human tumors: a review," *Cancer Res.* **49**(23), 6449–6465 (1989).
9. J. Xia, C. Wei, T.-M. Nguyen, B. Arnal, I. Pelivanov, and M. O'Donnell, "Clinically translatable integrated ultrasound and photoacoustic imaging system," in *SPIE BiOS*, 2014, p. 894310.
10. M. A. Lediju Bell, N. Kuo, D. Y. Song, and E. M. Boctor, "Short-lag spatial coherence beamforming of photoacoustic images for enhanced visualization of prostate brachytherapy seeds," *Biomed. Opt. Express* **4**(10), 1964–1977 (2013).
11. B. Pourebahimi, S. Yoon, D. Dopsa, and M. C. Kolios, "Improving the quality of photoacoustic images using the short-lag spatial coherence imaging technique," in *SPIE BiOS*, 2013, p. 85813Y.
12. S. Park, A. B. Karpouk, S. R. Aglyamov, and S. Y. Emelianov, "Adaptive beamforming for photoacoustic imaging using linear array transducer," in 2008 IEEE Ultrasonics Symposium, 2008, 1088–1091.
13. J. F. Synnevåg, A. Austeng, and S. Holm, "Adaptive Beamforming Applied to Medical Ultrasound Imaging," *IEEE Trans. Ultrason. Ferroelectr. Freq. Control* **54**(8), 1606–1613 (2007).
14. C. Yoon, Y. Yoo, T.-K. Song, and J. H. Chang, "Pixel based focusing for photoacoustic and ultrasound dual-modality imaging," *Ultrasonics* **54**(8), 2126–2133 (2014).

15. B. Lashkari and A. Mandelis, "Linear frequency modulation photoacoustic radar: optimal bandwidth and signal-to-noise ratio for frequency-domain imaging of turbid media," *J. Acoust. Soc. Am.* **130**(3), 1313–1324 (2011).
16. L. V. Wang and S. Hu, "Photoacoustic tomography: in vivo imaging from organelles to organs," *Science* **335**(6075), 1458–1462 (2012).
17. S. A. Telenkov and A. Mandelis, "Fourier-domain biophotoacoustic subsurface depth selective amplitude and phase imaging of turbid phantoms and biological tissue," *J. Biomed. Opt.* **11**(4), 044006 (2006).
18. S. A. Telenkov, R. Alwi, A. Mandelis, W. Shi, E. Chen, and A. I. Vitkin, "Frequency domain photoacoustic correlation (radar) imaging: a novel methodology for non-invasive imaging of biological tissues," in *SPIE BiOS*, 2012, p. 82231J.
19. Laser Institute of America, ANSI Z136.1–2007 American National Standard for Safe Use of Lasers. (2007).
20. B. Lashkari and A. Mandelis, "Comparison between pulsed laser and frequency-domain photoacoustic modalities: signal-to-noise ratio, contrast, resolution, and maximum depth detectivity," *Rev. Sci. Instrum.* **82**(9), 094903 (2011).
21. S. Telenkov, R. Alwi, A. Mandelis, and A. Worthington, "Frequency-domain photoacoustic phased array probe for biomedical imaging applications," *Opt. Lett.* **36**(23), 4560–4562 (2011).

1. Introduction

Over 585,000 cancer-related deaths are estimated in 2014 in the United States alone [1]. The early detection and treatment of cancer greatly increase the chances of survival [2]. Photoacoustic (PA) imaging is an emerging non-ionizing, non-invasive imaging modality being investigated for early cancer diagnosis [3,4]. It is based on the Photoacoustic (PA) effect – the generation of acoustic waves by the absorption of electromagnetic (EM) energy, which was first discovered by Alexander Graham Bell in 1880. PA imaging combines high optical contrast and spectroscopic-based specificity with high ultrasonic spatial resolution. The field of PA techniques has seen significant growth over the past decade in terms of instrumentation development, image reconstruction algorithms, in vivo applications in clinical medicine and basic biological research [5–7].

The abnormal growth of tumor cells (hypermetabolism) raises nutrients and oxygen consumption compared to normal tissue [8], thus resulting in the rapid development of dense microvascular network (i.e. angiogenesis), which is a critical indicator of the metabolic state of lesions. The sensitivity of PA imaging to oxygenated hemoglobin concentration can potentially quantify these hallmarks of cancer and facilitate its early detection through enhanced laser light absorption in the 650–1100 nm tissue optical window spectral range.

Ultrasound (US) imaging is widely used in clinical applications to detect tumors in patients [3,9]. Achieving PA imaging functionality on a commercial US instrument could therefore accelerate clinical acceptance and use. In PA imaging, the pressure waves generated in the photoacoustic effect can be detected by conventional US array transducers that convert the mechanical acoustic waves to electrical signals, making them highly compatible with US imaging. Obtaining both US and PA images, and by extension their co-registration, is simplified since the same transducer is employed for both modalities. Using existing commercial US array transducers is convenient, relatively inexpensive, and exploits advances made in diagnostic US imaging. US detectors, often piezoelectric-based having low thermal noise and high sensitivity, are capable of providing a wideband detection (up to 100 MHz [2]). Commercial US imagers also possess sophisticated software for rapid image acquisition which could potentially dramatically speed-up PA imaging, if developed to be compatible with that modality. Real-time hybrid (US-*pulsed* laser PA-based) imaging systems have been reported for human hand vasculature, sentinel lymph node detection in the breast (vital for determining the stage of breast cancer) and cardiovascular dynamics in small animals [5,6]. However, efficient PA and US integration and image co-registration is difficult as digital signal processing (DSP) in US imagers operates on *frequency-domain* (FD) principles. This renders the use of FD-PA imaging ("the photoacoustic radar" (PAR)) ideal for integrated image co-registration.

In this paper the integration of a frequency-domain photoacoustic radar (FD-PAR) imaging system and a portable commercial US imager (SonixTOUCH, Ultrasonix Medical Corp., Richmond, BC, Canada) is investigated. The system can provide separate and/or co-

registered US and PA images that can reveal (complementary) morphological information with comparable imaging axial resolution (\sim mm) and signal-to-noise ratio (SNR) to potentially facilitate early cancer detection. Image quality improvement has received a great deal of attention in PA with different techniques being explored, including short-lag spatial coherence [10,11], adaptive beamforming [12,13] and pixel based focusing [14]. The concept of phase filtering [15], through which PA signal spatial resolution can be improved by filtering the amplitude with the more localized phase, is introduced to PAR imaging.

2. PA radar imaging

PA imaging applies the PA effect to overcome limitations of optical imaging, including limited imaging depth with ballistic photons (approximately one photon mean free path (MFP) i.e. \sim 1 mm) or limited resolution with diffuse light (\sim 1 cm) [2,16] due to strong optical scattering in tissue causing spreading of light beams and loss of directionality, by converting optical to ultrasonic energy to take advantage of low acoustic scattering (2–3 orders of magnitude weaker than light scattering) in tissue. Upon illumination, biomolecules absorb photons, thermoelastically inducing pressure waves, and subsequently emitting less-scattering acoustic waves that are detectable at the tissue surface.

Unlike pulsed PA, FD-PA systems feature compact, inexpensive CW laser diodes with a wide wavelength selection (particularly, in the near-IR range) making them attractive for portable, sensitive PA imagers suitable for clinical applications. The FD-PAR imaging system developed at the Center for Advanced Diffusion-Wave Technologies (CADIFT) employs CW laser sources intensity-modulated (coded) and driven by frequency-swept (chirp) waveforms. The FD modality also possesses depth-selective imaging capabilities [17] and can generate high peak power cross-correlation response through matched filtering. Energy compression, typically, ms-long frequency chirps compacted into a narrow correlation peak, significantly increases SNR [18]. The reconstructed image is the spatial cross-correlation function between the PA response and the reference signal used for laser source modulation (the radar principle). SNR of FD-PA can also be greatly enhanced by coherently averaging multiple (typically 50–500) chirps and increasing laser power while congruently decreasing chirp duration (exposure), to remain within the maximum permissible exposure guidelines stipulated by regulatory bodies like the American National Standards Institute (ANSI) [19]. In principle, axial resolution in the pulsed mode is better due to larger bandwidth but the signal's bipolar shape is a downside. On the contrary, due to the lack of baseline oscillation in cross-correlation FD-PA and the ability to combine the FD phase signal with the amplitude signal, the FD mode has been shown to yield sub-mm axial resolution, better than or similar to, pulsed laser PA without the ultrasonic wake distortions which follow the laser pulse [20]. Additionally, FD-PA possesses superior contrast even after (high-pass) filtering is used to enhance the contrast of the pulsed response [20]. Using PAR can also help generate much higher image acquisition frame rates (kHz) than conventional nanosecond pulsed laser systems. Moreover, low peak-power CW laser irradiation of deeply embedded tumors is an added laser safety advantage.

Detailed descriptions of the basics of FD-PAR imaging are available elsewhere [21]. Image improvement techniques such as filtering using apodization functions as often done in conventional US imaging, and normalization, can be implemented. Furthermore, PAR produces two images (amplitude and phase-based) instead of one in pulsed PA imaging. This feature results in higher diagnostic reliability at each probed subsurface depth and phase can be used for further image improvement, as it tends to be more localized and of higher dynamic range (contrast) than amplitude. Phase contrast is more highly localized because phase lag is based on the energy centroid location of converted ultrasound through optical absorption across subsurface regions determined by the optical absorption depth. The PA ultrasonic centroid location does not depend on actual photon flux nor does it involve surface optical contrast due to reflection or absorption, unlike the PAR amplitude. As such the phase

lag is a truly photoacoustic imaging channel as opposed to a mixed PA and surface optical property image generated from the PAR amplitude [17]. Moreover, it does not depend on optical fluence, a major advantage over time-domain modalities. Phase-filtered imaging is, therefore, investigated as a spatial-resolution-improvement technique in this work. Amplitude (in-phase cross-correlation) and phase (the cross correlation of the detected signal with the quadrature of the input waveform) images are combined by filtering/multiplying the amplitude with the inverse of the standard deviation (SD) of the phase. The resultant envelope cross-correlation signal possesses higher contrast and spatial resolution than its separate parts. A smoother trace is also obtained, thereby diminishing the need for added FD windowing. However, combination amplitude – phase data acquisition and imaging takes longer than amplitude imaging alone, since the SD of the phase must also be recorded.

3. Experimental set-up and imaging procedures

Our system employs an 805-nm CW diode laser (Laser Light Solutions (LLS), NJ, USA) to illuminate the sample at an output power of 5W, and a standard commercial 64-element phased array transducer (Ultrasonix Medical Corp., Richmond, BC, Canada with 2 to 4 MHz frequency range and 0.254 mm pitch) to detect the PA signals generated. A power density of $\sim 1.59 \text{ W/cm}^2$ is obtained from the 5-W laser power illuminating over a 2-cm beam diameter, which is less than half of the calculated maximum permissible exposure (MPE) of 4.10 W/cm^2 for our CW system. Laser modulation was achieved by generating linear frequency modulated (LFM) chirp signals (0.5 to 4 MHz, 1-ms long) using a NI PXI-5442 (National Instrument, Austin, Texas) signal-generation card.

In vivo imaging of cancer cells injected into the left thigh of a nude mouse was performed. Human hypopharyngeal head and neck squamous cell carcinoma FaDu cell lines were obtained from the American Type Culture Collection (Manassas, VA), and cultured in MEM F-15 supplemented with 10% fetal bovine serum. 1×10^7 cultured cells were injected into the left thigh of the mouse, three weeks prior to imaging. The animal was fully anesthetized throughout the experiment by administering 1.4 L/min of oxygen and 1 L/min of isoflurane gas. An IR lamp and a heating and temperature controller were used to regulate the animal body temperature (at a constant level). The experiment was performed under the guidelines of animal protocol 20010465 approved by the Division of Comparative Medicine (DCM) of the Faculty of Medicine, University of Toronto. Animal handling was also performed according to guidelines for laboratory animal care.

A schematic of the experimental set-up is shown in Fig. 1. The sample and transducer surfaces were fully-submerged in water for acoustic coupling. Sequential data acquisition and signal processing were performed using modular analog-to-digital converters, Lab View (National Instruments, Austin, Texas) [21], and Matlab software. Using four programmable switch boards, an economical and flexible architecture was achieved through a synthetic receive aperture and multiplexer system. It allows for parallel readout of a subarray of eight elements sequentially multiplexed over the entire array in reasonable time. Increasing the subarray size and total number of channels is also possible due to the ease of hardware expansion permitted by its modularity.

Amplitude data acquisition took ~ 320 ms. To perform consecutive imaging, the laser should be off 55% of the time, meaning a 392 ms relaxation time for each 320 ms of exposure. This results in a frame rate of ~ 1.40 Hz. The frame rate can be improved for real-time imaging (i.e. ~ 25 Hz) by using additional National Instrument (NI) cards for data collection. PA image reconstruction was done by a FD beamforming algorithm similar to that employed in conventional US images making it adequate for integration with clinical US systems for co-registration.

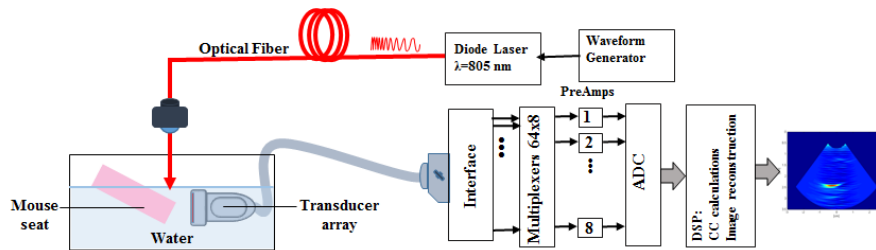


Fig. 1. Schematic of experimental set-up.

To find the tumor inside the thigh, the transducer placed in front of the thigh and the laser beam were moved in tandem along the body part and PA images were produced. Upon finding the tumor location, the transducer was adjusted to optimize the image. The tumor was located less than 3 mm below the skin, based on visual inspection of the tumor after euthanasia. Measurements were performed at three laser energy levels (3 W, 4 W, 5 W) including scans of the region of interest (ROI) at 5 W. The images obtained are consistent. As the transducer was fixed by connecting the zero insertion force (ZIF) connector to the Ultrasonix system, the US image was also produced at the same location, ideal for spatial co-registration of the two modalities, with the US image providing structural guidance to the PA image and tumor location information with respect to its surrounding tissues. The effectiveness of the phase-filtered imaging technique was also demonstrated via this experiment.

4. Results and discussion

To confirm the presence of the tumor in the left thigh of the mouse, histological validation was performed. Hematoxylin and eosin (H&E) staining was performed on the removed tissue and the stained sections were reviewed under a microscope with x200 magnification as shown in Fig. 2. H&E staining of the tissue reveals a high density of cancer cells that possess dark nuclei (Fig. 2(a)) while normal tissues (Fig. 2(b)) are seen as the (clear) pink sections, illustrating the presence of the tumor interlaced with the surrounding normal muscle tissue. This leads us to hypothesize that the cancer may have increased overall vascularity of the area of interest.

A photograph of the position of the mouse placed in its seat, relative to the transducer, is provided in Fig. 3(a). The tumor region is identified with the red circle. The pure US image of the cancer cell-injected mouse was obtained from the SonixTOUCH US imager at a frequency of 4 MHz as shown in Fig. 3(b). The tumor is difficult to distinguish among all other body parts reflecting the US such as bone, muscle and fat (indicated by the dashed oval). The bright spot shown by the white arrow is suspected to be the bottom of the plastic seat for the mouse.

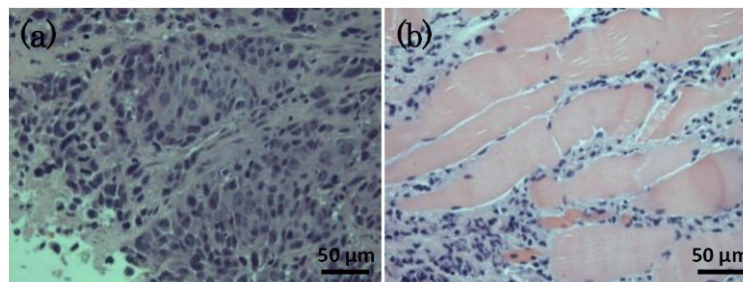


Fig. 2. Xenografts of cancer cells with dark nuclei (a) and normal tissue (b).

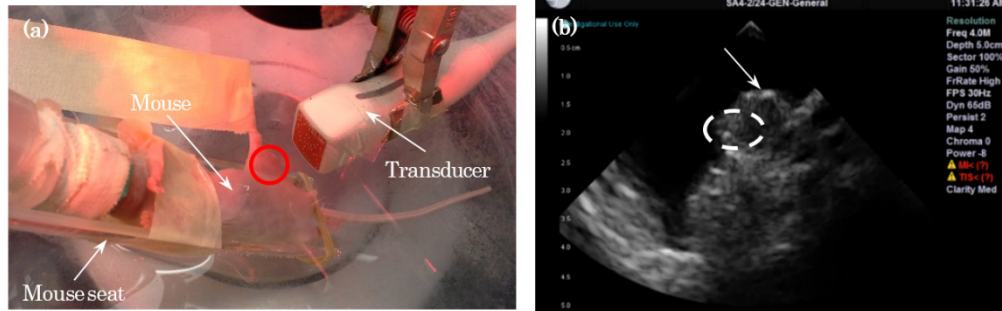


Fig. 3. (a) Experimental set-up showing mouse secured to the seat and the transducer positioned in front of it. (b) Pure US image obtained from commercial Ultrasonix imager.

On the contrary, the reconstructed PAR images in Fig. 4(a) clearly indicate the location of the absorber (tumor) at $\sim 1.7\text{--}2.2$ cm from the transducer surface. Unlike the US image, the PA image is less sensitive to the presence of the surrounding body parts, but is highly sensitive to the presence of increased blood flow in the tumor, thereby providing much clearer information regarding the tumor, manifested as better contrast and sensitivity than its pure US counterpart. Figures 4(a), 4(b), 4(c) show the amplitude (see [18] for methodology), phase only and phase-filtered images, respectively, obtained by the PAR system.

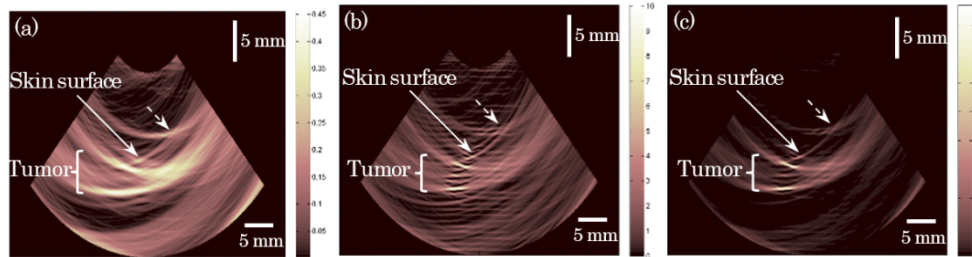


Fig. 4. Amplitude (a), Phase (b) and Phase-filtered (c) PAR images of the left mouse thigh.

The phase image (Fig. 4(b)) shows a more localized tumor with better contrast than the amplitude image while an even more improved image is obtained in the phase-filtered image (Fig. 4(c)), evaluated by filtering the amplitude with the inverse of the SD of the phase. The tumor in the phase-filtered image seems just as localized and particularly more accentuated (higher contrast) due to the suppressed background noise resulting from phase-filtering. The dashed arrows in the PA images of Fig. 4 are placed at locations suspected to be blood vessels on the back of the mouse.

To understand the effectiveness of phase-filtered PAR imaging, cross-correlation signals (A-scans) corresponding to amplitude and phase PA images in Fig. 4 are shown in Fig. 5 where the strong signal amplitude (at $\sim 13\text{-}\mu\text{s}$ delay time) indicates the presence of the tumor. The peak at $\sim 10\text{-ms}$ delay is the element's view of microvasculature near the back of the mouse (toward the tail). The A-scan for the phase illustrates its superior localization relative to the amplitude with narrower peaks seen at corresponding delay times. This was further confirmed by performing a scan of the mouse thigh which revealed similar increased signal strength at that same location when it was put within the range of the transducer. The spatial extent of the tumor is further represented in the images provided.

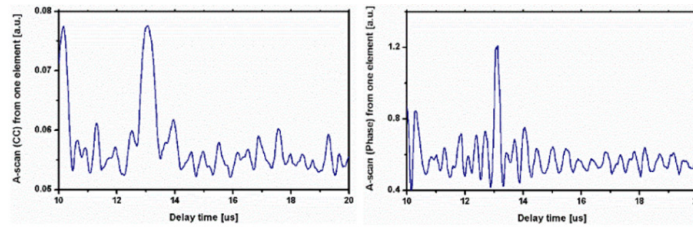


Fig. 5. Amplitude (left) and Phase (right) cross-correlation signal from one element of the transducer over tumor location.

From the cross-correlation (PA response) data obtained from the experiment, the SNR for the phase-filtered image shows a 14 dB and 15 dB increase over the amplitude and phase alone, respectively. Spatial resolution is estimated from the full-width at half maximum (FWHM) of the signal to be $\sim 840 \mu\text{m}$ for amplitude PAR and improved to $\sim 340 \mu\text{m}$ for the corresponding phase PAR.

Figure 6 provides the co-registered US and PA phase images. Tumor information obtained in the phase-filtered PAR image is overlaid on the US image to provide enhanced tumor diagnostics (higher diagnostic power). The zoomed image (Fig. 6(b)) of the ROI in Fig. 6(a), indicates the position of the tumor relative to the other body parts delineated in the US image and illustrates the spatial extent of the tumor.

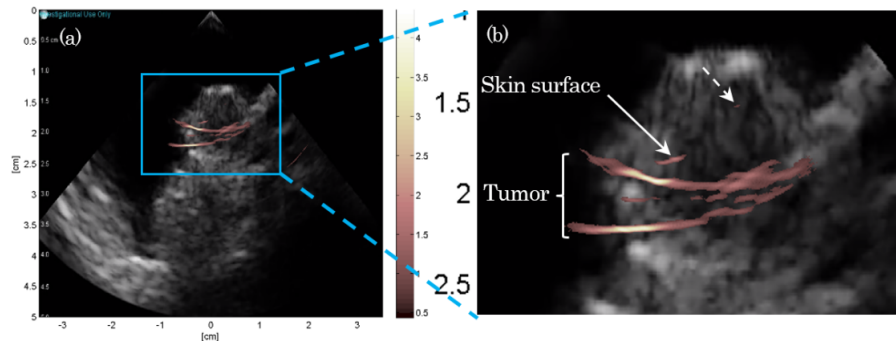


Fig. 6. (a) Phase-filtered PAR image superimposed on the pure US image of the left thigh of the mouse. (b) Zoomed image of the region of interest.

5. Conclusions

The present work demonstrates the co-registration of US and FD-PAR images with significant image improvement from leveraging the phase information obtained in PAR imaging.

Experimental results presented demonstrate live animal testing and show enhancements in SNR, contrast and spatial resolution (providing clearer information regarding the tumor) via phase-filtered PAR imaging owing to the high localization of the phase. Applying sophisticated US-inspired software could speed-up PA imaging and offset the slower phase-filtered data acquisition. Co-registration of US and PAR phase images, works cooperatively toward the optimization of spatial resolution and image acquisition speed than either modality independently. Further studies are underway to fully amalgamate both US and PAR modalities into a single imager.

Acknowledgments

A.M. is grateful to the Natural Sciences and Engineering Research Council of Canada (NSERC) for a Discovery Grant and to Samsung Advanced Institute of Technology (SAIT) through a Global Research Outreach (GRO) Research Project Grant.